

Synthesizing Diverse and Physically Stable Grasps with Arbitrary Hand Structures by Differentiable Force Closure Estimation

Tengyu Liu¹, Zeyu Liu¹, Ziyuan Jiao¹, Yixin Zhu¹, Song-Chun Zhu¹

Abstract—Existing grasp synthesis methods are either analytical or data-driven. The former one is oftentimes limited to specific application scope. The latter one depends heavily on demonstrations [1], thus suffers from generalization issues; *e.g.*, models trained with human grasp data would be difficult to transfer to 3-finger grippers. To tackle these deficiencies, we formulate a fast and differentiable force closure estimation method, capable of producing diverse and physically stable grasps with *arbitrary* hand structures, *without any training data*. Although force closure has commonly served as a measure of grasp quality, it has not been widely adopted as an optimization objective for grasp synthesis primarily due to its high computational complexity; in comparison, the proposed differentiable method can test a force closure within 4ms. In experiments, we validate the proposed method’s efficacy in 8 different settings.

I. INTRODUCTION

Grasp synthesis has been a challenging task due to the complexity of hand kinematics. Although force closure has been commonly accepted to evaluate the quality of the generated grasps, researchers usually avoid using it as an optimization objective: Computing force closure requires solving for contact forces, which is an optimization problem itself. As a result, using force closure as the optimization objective in grasp synthesis would produce a notoriously slow and nested optimization problem. Instead, researchers have turned to analytical or data-driven methods [1].

Analytical methods use manually derived algorithms. Due to the intrinsic complexity of the grasp synthesis, these methods [2–4] typically perform only in limited settings (usually on power grasps as defined in grasp taxonomy) and are only applicable to specific robotic hand structures. Modern approaches focus more on data-driven methods [5–7], which relies on large datasets of human demonstrations. Although these methods are able to reproduce (and even interpolate) similar but different grasps compared to human demonstrations, they are inherently difficult to generalize (especially to extrapolate) to arbitrary hand kinematics and unseen grasp types. Furthermore, these data-driven methods usually do not consider the physical stability in producing grasps, making them difficult to deploy on physical robots.

In this paper, different from analytical or data-driven approaches, we derive a fast and differentiable estimation of force closure. It can be computed within **milliseconds** on modern desktops, significantly faster than classic algorithms. Such fast computation of force closure opens a new venue

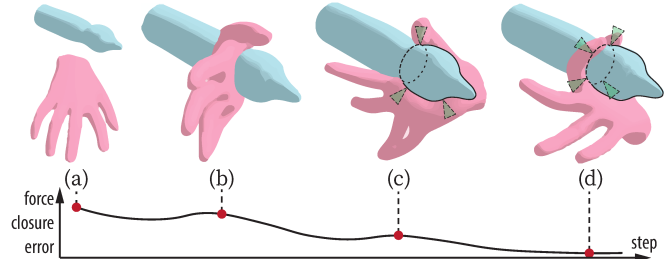


Fig. 1: Grasp synthesis process by minimizing force closure error. The green trianglelets in (c)(d) denote the friction cones at contact points used to calculate force closure.

for grasp synthesis. Since it does not rely on training data or restrict to specific robotic hand structures, the proposed method can be applied to arbitrary hand structures to synthesize diverse types of grasps with physical stability.

Specifically, our method is based on two simple yet reasonable and effective assumptions: **zero friction** and **equal magnitude of contact forces**, which avoid solving the contact forces in the inner optimization problem. Intuitively, such assumptions indicate that the contact force on each contact point becomes simply the object’s surface normal on that point. As such, the overall nested optimization problem is converted to minimizing the errors that violate the above assumptions; see an example in Fig. 1. In experiments, we demonstrate that our estimated error reflects the difference between surface normal vectors and force closure contact force vectors. We further devise a grasp energy function based on the estimated force closure and validate the force-closure grasp synthesis by minimizing the energy function.

This paper makes two primary contributions:¹

- 1) We formulate a fast and differentiable estimation of force closure, computed within milliseconds.
- 2) We propose a grasp synthesis algorithm that can generate diverse types of grasps with arbitrary hand structures without any training data.

II. RELATED WORK

Grasp synthesis literature can be roughly categorized into two schools of thought: analytic and data-driven approach.

The analytic approach generates grasps by considering kinematics and physics constraints [8]. Although force closure has been commonly adopted as the physics constraint [9–12], primary efforts have been devoted to simplify the search space (*e.g.*, [2–4]) as testing force closure is

¹ UCLA Center for Vision, Cognition, Learning, and Autonomy (VCLA). Emails: {tengyuliu, lzy, zyjiao, yixin.zhu}@ucla.edu, sczhu@stat.ucla.edu.

The work reported herein was supported by ONR N00014-19-1-2153, ONR MURI N00014-16-1-2007, and DARPA XAI N66001-17-2-4029.

¹See additional material on our website <https://sites.google.com/view/ral2021-grasp/>.

expensive. However, these methods are only effective in specific settings.

The data-driven approach leverages recent advancements in machine learning to estimate grasp points. Despite promising progress [13–18], this approach relies heavily on large datasets to learn successful grasps, with a particular focus on grippers with limited DoF. Although recent literature [19–22] extends this approach to more complex hand models, capable of generating more realistic grasps, they still rely on the expensive and tedious collection of human demonstration data. Fundamentally, it is non-trivial for a data-driven approach to generalize the learned model to other hand kinematics.

An example that does not fall into either of the above categories is the popular toolkit of GraspIt! [23]. It generates grasps by initializing hand pose randomly, squeezing the fingers as much as possible, and ranking them by a user-defined grasp metric (*e.g.*, a force closure metric). Although this method can generate valid grasps, it is highly inefficient and incapable of generating diverse grasps [24].

A **force-closure** grasp is a grasp with contact points $\{x_i \in \mathbb{R}^3, i = 1, \dots, n\}$ such that $\{x_i\}$ can resist arbitrary external wrenches with contact forces f_i , where f_i lies within the friction cones rooted from x_i . The angles of the friction cones are determined by the surface friction coefficient: The stronger the friction, the wider the cone. The force-closure metric is, therefore, irrelevant to the actual hand pose, but only relevant to the contact points and friction cones.

To test whether a set of contact points form a force-closure grasp, the first step is solving an optimization problem regarding contact forces rooted from the points [25, 26]. Although various methods have been devised, they all require iterations to jointly solve an auxiliary function, *e.g.*, a support function [27], a bilinear matrix inequality [28], or a ray shooting problem [29]. As a result, solving force-closure grasps under the constraint of hand kinematics and force closure becomes a nested optimization problem.

Human grasps can be organized into a **grasp taxonomy** [30]; humans perform grasps to provide different levels of power and precision. According to the taxonomy [30], most existing grasp synthesis methods focus on synthesizing power grasp, including both analytical approaches [9–12] and data-driven approaches [7]. At a high cost of annotating object-centric grasp contact information, some data-driven approaches [5, 21] demonstrate a certain level of capability to generate a broader range of grasp types.

The diversity of grasp synthesis can be evaluated by comparing the types of generated grasps against the ones in the grasp taxonomy. Corona *et al.* [24] provide a dataset, YCB-Affordance, of 3D grasps with corresponding grasp types, which covers all 33 grasp types as defined in [30].

III. DIFFERENTIABLE FORCE CLOSURE

Formally, given a set of n contact points $\{x_i \in \mathbb{R}^3, i = 1, \dots, n\}$ and their corresponding friction cones $\{(c_i, \mu)\}$, where c_i is the friction cone axis and μ is the friction coefficient, a grasp is in *force closure* if there exists contact forces $\{f_i\}$ at $\{x_i\}$ within $\{(c_i, \mu)\}$ such that $\{x_i\}$ can resist

arbitrary external wrenches. We follow the notations in Dai *et al.* [28] to define a set of contact forces to be force closure if it satisfies the following constraints:

$$GG' \geq \epsilon I_{6 \times 6}, \quad (1a)$$

$$Gf = 0, \quad (1b)$$

$$f_i^T c_i > \frac{1}{\sqrt{\mu^2 + 1}} |f_i|, \quad (1c)$$

$$x_i \in S, \quad (1d)$$

where S is the object surface, and

$$G = \begin{bmatrix} I_{3 \times 3} & I_{3 \times 3} & \dots & I_{3 \times 3} \\ [x_1]_{\times} & [x_2]_{\times} & \dots & [x_n]_{\times} \end{bmatrix}, \quad (2)$$

$$[x_i]_{\times} = \begin{bmatrix} 0 & -x_i^{(3)} & x_i^{(2)} \\ x_i^{(3)} & 0 & -x_i^{(1)} \\ -x_i^{(2)} & x_i^{(1)} & 0 \end{bmatrix}. \quad (3)$$

The form of $[x_i]_{\times}$ ensures the cross product $[x_i]_{\times} f_i = x_i \times f_i$; $f = [f_1^T f_2^T \dots f_n^T]^T \in \mathbb{R}^{3n}$ is the unknown variable of contact forces. In Eq. (1a), ϵ is a small constant. $A \geq B$ means $A - B$ is positive semi-definite, *i.e.*, it is symmetric, and all its eigenvalues are non-negative. Eq. (1a) states that G is full rank. Eq. (1c) describes the constraint that f_i should not deviate from the friction cone $\{(c_i, \mu)\}$.

A. Relaxation

Of note, Eq. (1b) is bilinear on x_i and f_i . Given a set of contact points $\{x_i\}$, verification of force closure requires finding a solution of $\{f_i\}$. The time complexity for computing such a solution is linear w.r.t. the number of contact points [28]. However, we observe that under the assumption of zero friction and the contact forces have equal magnitude, Eq. (1b) can be relaxed and rewritten to

$$GG' \geq \epsilon I_{6 \times 6}, \quad (4a)$$

$$Gc < \delta, \quad (4b)$$

$$x_i \in S, \quad (4c)$$

where $c = [c_1^T c_2^T \dots c_n^T]^T$ is the set of friction cone axes; c_i can be simply replaced by the surface normal of the object on x_i , which is easily accessible in many shape representations. By combining Eq. (4b) along with Eq. (1a) and Eq. (1c), we no longer need to solve the unknown variable f . The constraints of x_i becomes quadratic. Hence, the verification of force closure can now be computed extremely fast. The error in Gc reflects the difference between force closure contact forces and friction cone axes.

B. Implications of Assumptions

Enforcing zero friction and equal magnitude contact forces may *seem* to eliminate a large pool of force-closure contact-point compositions. In practice, however, this is not the case: A residual in $\|Gc\|_2$ indicates that the zero-friction and equal-magnitude contact forces do not perfectly cancel out. Such residual could have been reduced to zero should friction and magnitude difference be allowed. Fig. 2 illustrates the implication of our assumptions in 2D. Specifically, for cases where our assumptions are violated, $\|Gc\|_2$ would have a

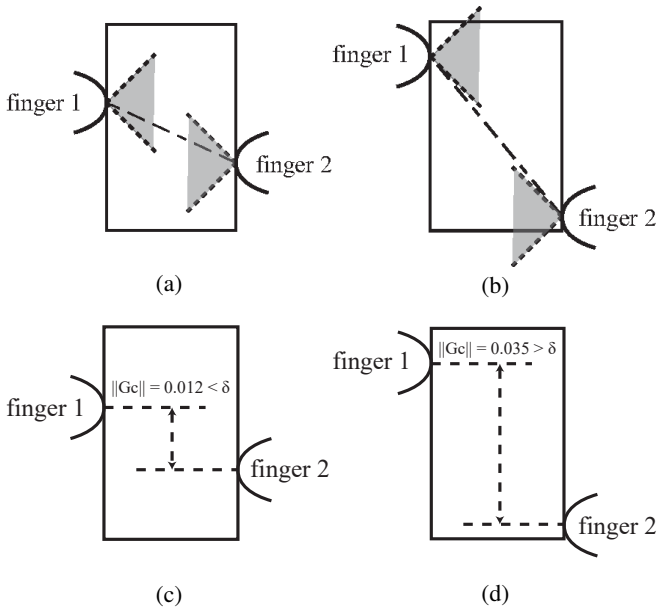


Fig. 2: **A 2D illustration of the classical force closure test and our estimated force closure error.** (a)(b) Two scenarios passed and failed the classical force closure test. (c)(d) Our estimated force closure error on the same scenarios as in (a)(b).

non-zero error δ . Eq. (1b) can be rewritten as

$$Gf = G(f_n + f_t) = 0, \quad (5a)$$

$$G \frac{f_n}{\|f_n\|_2} = - \frac{Gf_t}{\|f_n\|_2}, \quad (5b)$$

$$Gc = - \frac{Gf_t}{\|f_n\|_2}, \quad (5c)$$

where f_n and f_t are the normal and tangential components of contact force f in the force closure model. Having an error in $\|Gc\|_2$ essentially implies that there is a friction components in the contact forces to form a force closure grasp, and the error δ indicates the magnitudes of the friction components.

To further verify our interpretation, we randomly sample 500,000 grasps, each containing three contact points on the surface of a unit sphere. For each grasp, we compute the *minimum* friction coefficient μ_0 required for the grasp to satisfy the traditional force closure constraints described in Eq. (1). We plot the error δ of our estimated force closure value against μ_0 in Fig. 3 to show that the relation between μ_0 and δ is almost linear.

IV. GRASP SYNTHESIS

A. Formulation

We formulate the grasp synthesis problem as sampling from a conditional Gibbs distribution:

$$P(H|O) = \frac{P(H|O)P(O)}{P(O)} = \frac{P(H,O)}{P(O)} \quad (6)$$

$$\propto P(H,O) = \frac{1}{Z} \exp^{-E(H,O)}, \quad (7)$$

where H denote the hand, O the object, Z the intractable normalizing constant, and $E(H,O)$ is the grasp energy.

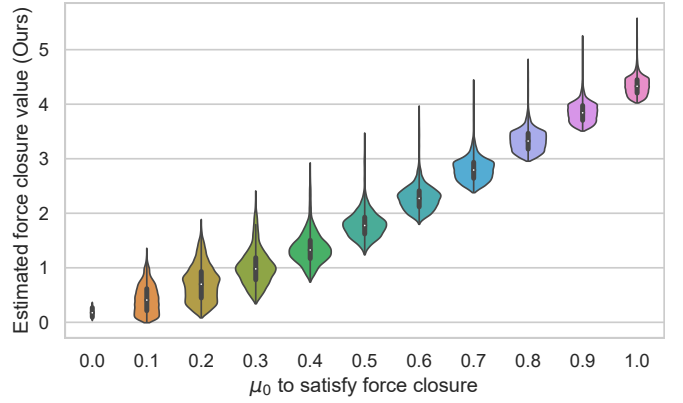


Fig. 3: **Estimated force closure error δ (x-axis) against minimum friction coefficient μ_0 (y-axis).** The violinplots [31] show the distributions of all estimated force closure errors that require a minimum friction coefficient μ_0 to pass the classical force closure test. Overall, these two are linearly correlated.

$E(H,O)$ can be further decomposed to

$$E(H,O) = \min_{x \in S(H)} E_{grasp}(H,x,O) \quad (8)$$

$$= \min_{c \in S(H)} FC(c,O) + E_{prior}(H) + E_{pen}(H,O), \quad (9)$$

where $S(H)$ is a set of points sampled from the hand surface determined by the hand pose H , $c \in S(H)$ the set of contact points selected from hand surface, and $FC(c,O)$ the force closure formulation from Eq. (11).

$E_{prior}(H)$ is the *energy prior* of the hand kinematic tree; its exact form depends on the hand definition. $E_{pen}(H,O)$ is the *penetration energy*, defined as $E_{pen}(H,O) = \sum_{x \in S(H)} \sigma(x,O)$, where $S(H)$ is a set of points sampled from hand surface, and $\sigma(x,O)$ is a modified distance function between a point x and an object O :

$$\sigma(x,O) = \begin{cases} 0 & \text{if } x \text{ outside } O \\ |d| & \text{otherwise} \end{cases}, \quad (10)$$

where d is the distance from x to surface of O .

B. Algorithm

Due to the complexity of human hand kinematics, the landscape of our grasp energy is highly non-convex. With a naive gradient-based optimization algorithm, it is very likely to get stuck at bad local minima. We use a modified Metropolis-adjusted Langevin algorithm (MALA) to overcome this issue; see the algorithm details in Algorithm 1. The random walk aspect of Langevin dynamics provides the chance of escaping bad local minima. Our algorithm starts with random initialization of hand configuration H and contact points $c \in S(H)$. Next, we run our algorithm L iterations to update H, c and maximize $P(H,O)$. In each iteration, our algorithm randomly decides to update either the hand configuration by Langevin dynamics or one of the contact points to a point uniformly sampled from the hand surface.

To sample contact points from the hand surface, we start with random initialization of contact points, and randomly update one of the contact points to a point uniformly sampled from the hand surface each time. Notice that different compo-

sitions of contact points in fact correspond to different grasp types as they contribute to some of the classification basis of the grasp taxonomy, including virtual finger assignment and opposition type. Hence, this step is crucial for exploring different types of grasps. In practice, we also empirically find that this step is crucial for escaping bad local minima.

Algorithm 1: Modified MALA Algorithm

Input: Energy function E_{grasp} , object shape O , step size η , Langevin steps L , switch probability ρ

Output: grasp parameters H, c

```

1 Initialize  $H, c$ 
2 for  $step = 1 : L$  do
3   if  $rand() < \rho$  then
4     Propose  $H^*$  according to Langevin dynamics
       
$$H^* = H - \frac{\eta^2}{2} \frac{\partial}{\partial H} E_{grasp}(H, c, O) + \eta \epsilon,$$

       where  $\epsilon \sim N(0, 1)$  is a Gaussian noise
5   else
6     Propose  $c^*$  by sampling from  $S(H)$ 
7   end
8   Accept  $H \leftarrow H^*, c \leftarrow c^*$  by Metropolis algorithm
   using energy function  $E_{grasp}$ 
9 end

```

C. Refinement

While our modified MALA algorithm can produce realistic results, there may still be physical inconsistencies in the synthesized examples, such as penetrations and gaps between contact points and object surface. To resolve these issues, we further refine the synthesized results by minimizing E_{grasp} using gradient descent on H . We do not update the contact point selection c in this step since we hope to focus on optimizing the physical consistency in this step, rather than exploring the grasp landscape for diverse grasp types.

V. EXPERIMENT

A. Experiment Setup

Hand Model: We use MANO [32] to model the humanoid hand. It is a parameterized 3D hand shape model that maps low-dimensional hand poses to 3D human hand shapes. We use the norm of the PCA weights of the hand pose as $E_{prior}(H)$. Since MANO vertices are distributed uniformly across the hand surface, we sample points from the hand surface by directly sampling from MANO vertices.

Object Model: We use the DeepSDF model [33] to model the objects to be grasped. DeepSDF is a densely connected neural network that implicitly represents the surface of a shape. The model estimates the signed distance from a position to an object surface. The signed distance is negative if the point is inside the object, and is positive if the point is outside the object. The set of points with zero distance compose the surface of the object. We can obtain the surface normal of the object by taking the derivative of the signed distance w.r.t. the input position.

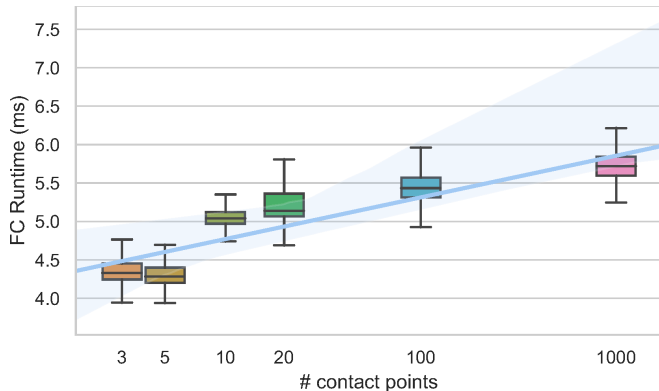


Fig. 4: **Boxplot and log-linearly fitted curve of the runtime w.r.t. to the number of contact points.** We run a simulated test of force closure with 3, 5, 10, 20, 100, and 1000 contact points for 1,000 iterations. X-axis is the number of contact points in log scale. Y-axis is the runtime of our force closure error estimation. The shaded area denotes the 95% confidence interval.

B. Runtime Efficiency

Figure 4 shows that the time complexity of testing force closure with a fitted log-linear curve w.r.t. the number of contact points. Each test takes 4-6ms to run on an NVIDIA Titan RTX GPU, significantly faster than the exact solution [28]. We also observe that roughly 80% of the total runtime is spent at the computation of surface normal; this operation is particularly slow because it takes a derivative of the DeepSDF model. Taken together, these empirical simulated results indicate that a further improvement in runtime efficiency would be achievable with a more computationally tractable object shape representation.

C. Force-closure Contact-point Generation

By directly minimizing the proposed force closure estimate, we can synthesize force closure contact points with arbitrary shapes. Specifically, we rewrite the solution of constraint in Eq. (4) as

$$x^* = \arg \min_x FC(x, O),$$

$$FC(x, O) = \lambda_0(GG' - \epsilon I_{6 \times 6}) + \|Gc\|_2 + w \sum_{x_i \in x} d(x_i, O), \quad (11)$$

where G is defined in Eq. (2), and $c = \{c_i\}$, where c_i is the surface normal of object O at point x_i . $\lambda_0(\cdot)$ gives the smallest eigenvalue. $d(x, O)$ returns the distance from point x to the surface of object O . w is a scalar that controls the weight for the distance between contact points and object. By minimizing the three terms, we are looking for $\{x_i\}$ that satisfies the constraints in Eqs. (4a) to (4c), respectively.

We run gradient descent on contact point positions to minimize $FC(x, O)$; the computed contact points on a unit sphere and some daily objects are shown in Fig. 6. Despite our assumptions, minimizing our force closure estimate can properly produce force closure contact points.

D. Grasp Synthesis

We test our grasp synthesis algorithm on various bottles retrieved from ShapeNet dataset [34]. Given the pre-trained DeepSDF model of an object, we randomly initialize a

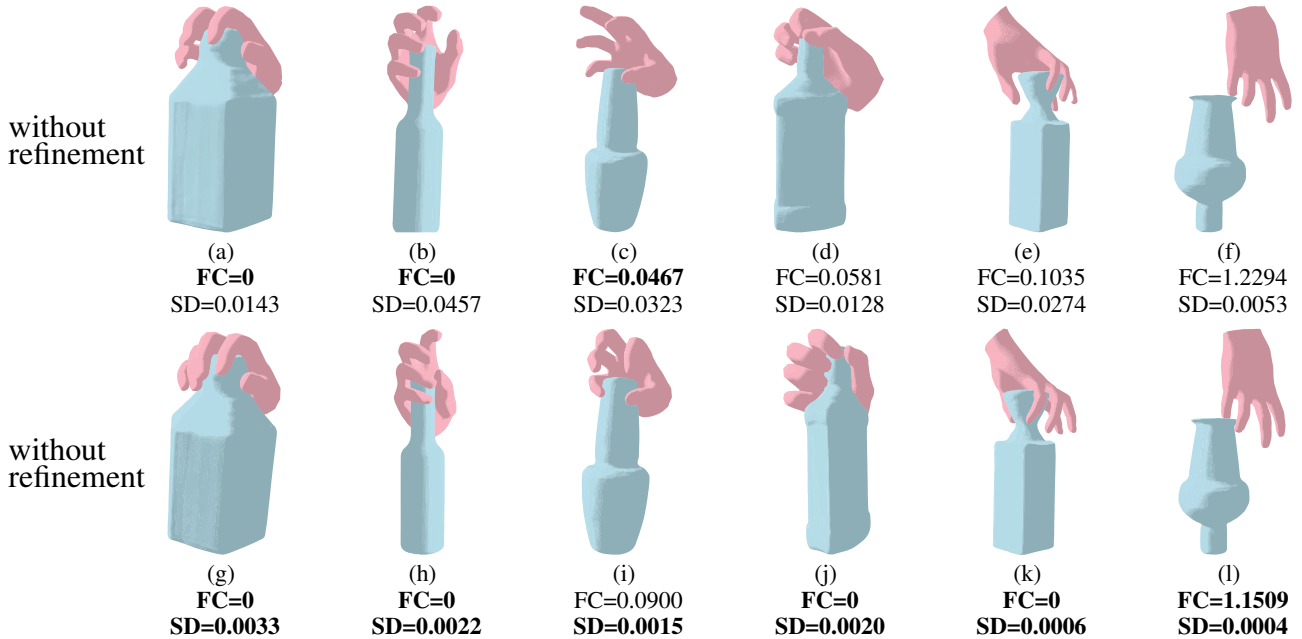


Fig. 5: **Examples of synthesized grasps.** Top: synthesized grasps before refinement. Bottom: the same set of synthesized grasps after refinement. FC: estimated force closure error. SD: mean distance from each contact point to the object surface. Left to right: examples with zero FC error, small FC error, and high FC error qualitatively illustrate how our estimation of force closure correlates to grasp quality.

MANO hand and use Algorithm 1 to sample the hand configuration as well as contact points from $P(H|O)$. We set the step size $\eta = 0.1$, switch probability $\rho = 0.85$, distance weight $w = 1$, temperature $T = 0.1$, and Langevin steps $L = 10^6$. We filter out samples trapped in bad local minima by keeping samples that satisfy the constraint:

$$\|Gc\|_2 < 0.5 \quad (12a)$$

$$\sum_{x_i \in x} d(x_i, O)^2 < 0.02 \quad (12b)$$

$$E_{pen}(H, O) < 0.02 \quad (12c)$$

where x is the set of contact points on the hand surface, and c is the friction cone axes at contact points. Fig. 5 shows a collection of synthesis results with and without the refinement step: Higher values of our force closure estimation corresponds to non-grasps, whereas force closure estimation closed to zero is as good as the ones with force

closure estimation equal to zero. **This observation confirms our previous analysis.** We also notice cases when the synthesis is trapped in bad local minima; these examples exhibit large values in our force closure estimation. We show two examples in the last column of Fig. 5. Such errors happened since the optimization problem is highly non-convex; one cannot avoid every bad minimum with gradient-based methods. Fortunately, we can identify these examples by their high force closure scores.

E. Physical Stability

We verify the physical stability of our synthesized examples by simulating the samples in PyBullet. Specifically, we set gravity to be $[0, 0, -10]$; an example is deemed to be a successful grasp if the object’s vertical drop is less than 0.3 after 1000 steps of simulation. Notice that a grasp’s physical stability depends not only on the force closure score of the contact points, but also on whether the contact points are close enough to the object surface. We set two different thresholds on the contact point distance; Table I tabulates detailed comparisons of the success rate between our method against state-of-the-art algorithms [36, 37]. To the best of our knowledge, [36] is the state-of-the-art analytic approach, whereas [37] is the state-of-the-art data-driven approach. Of note, although [37] reported 95% success rate in the original paper, many of the objects being tested have simple shapes, such as a sphere or a box; the success rate would drop to 85% when we remove these simple objects. Additionally, neither of the two state-of-the-art methods has demonstrated the ability to synthesize diverse types of grasps. Although some other data-driven methods have demonstrated a certain level of diverse grasp synthesis, they fail to report their physical stability as it is not their primary focus.

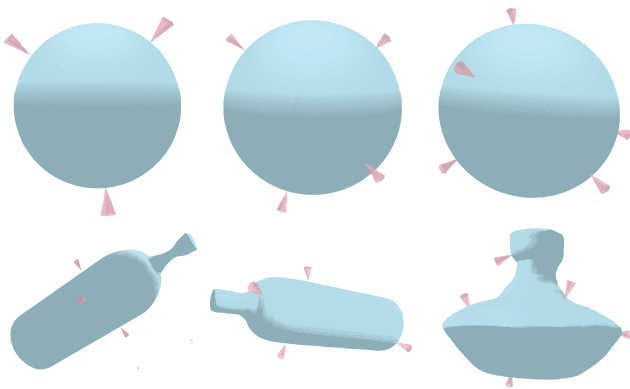


Fig. 6: **Force-closure contact-point generations on unit spheres (top) and daily objects (bottom) by minimizing Eq. (11).** Objects in each columns have 3, 4, and 5 contact points, respectively.

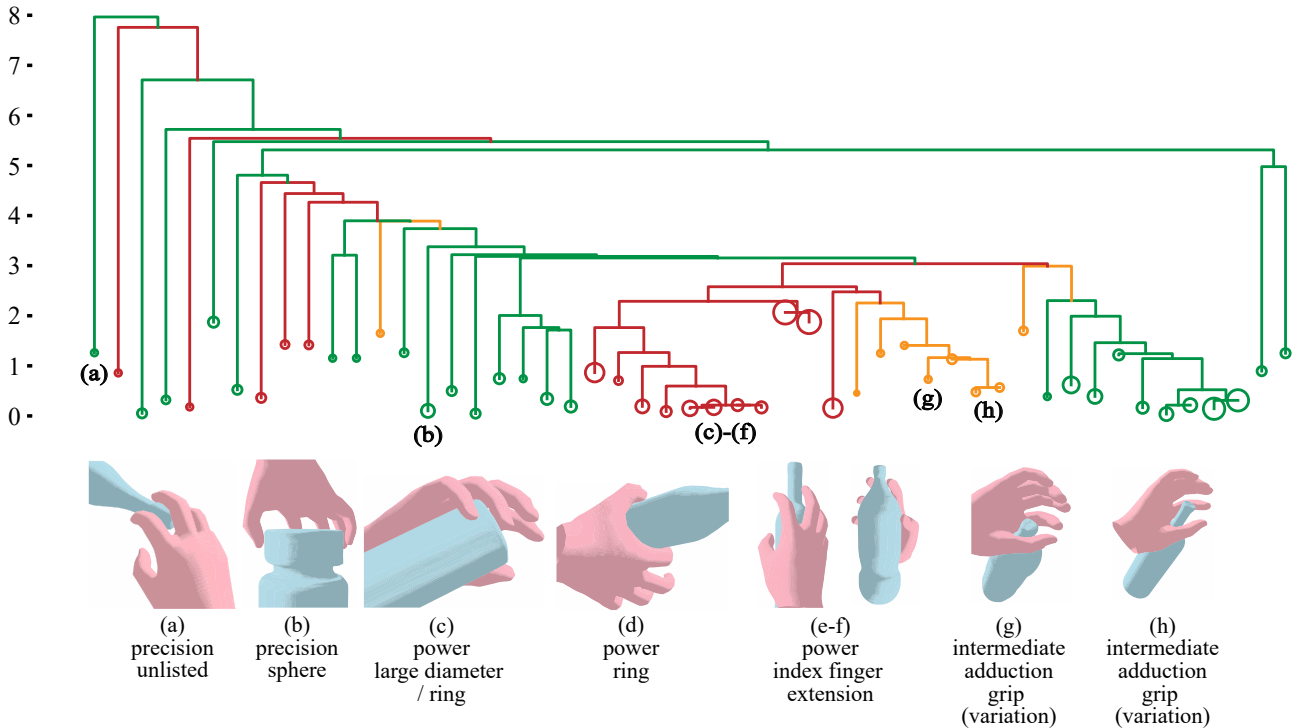


Fig. 7: **Energy landscape mapping generated by the ADELM algorithm [35] (best viewed in color)**. Top: disconnectivity diagram of the energy landscape of our energy function $E(H, O)$. Green minima denote precision grasps, red power grasps, and yellow intermediate grasps. Bottom: examples from selected local minima; minima with lower energy barriers in between have similar grasps. We also label the grasp taxonomy of each example according to [30]. Examples marked as *unlisted* do not belong to any manually classified type.

TABLE I: Grasp success rates

method	success rate
Unions of Balls [36]	72.53%
Visuo-Haptic [37]	85.00%
Ours ($\sigma < 0.0015$)	76.98%
Ours ($\sigma < 0.0005$)	85.00%

F. Diversity of the Grasp Types

To evaluate the grasp synthesis’s diversity generated by the proposed method, we examine the energy landscape of our grasp energy function. Below, we show that the distribution of grasps defined by our energy function loosely aligns with the carefully organized grasps taxonomy [30] when applied to humanoid hands. We use the ADELM algorithm [35] to build the energy landscape mapping of our grasps energy function $E(H, O)$.

Specifically, we collected 371 synthesized grasp examples and adopted the ADELM algorithm [35] to find minimum energy pathways (MEPs) between them. We project the MEPs between examples to a disconnectivity graph in Fig. 7. In the disconnectivity graph, each circle at the bottom represents a local minima group. The size of the circle indicates how many synthesized examples fall into this group. The height of the horizontal bar between two groups represent the maximum energy (or energy barrier) along the MEPs between two groups. The MEPs with lowest barriers connect smaller groups into larger groups, and this process is repeated until all examples are connected. The produced disconnectivity graph is an estimation of the true landscape of the energy

function. Energy landscape mapping in Fig. 7 shows that the local minima with low energy barriers between them have similar grasps, and those with high energy barriers between them tend to have different grasps. We also observe that the energy landscape contains all three categories in the power/precision dimension as described in [30].

To provide a more comprehensive understanding of the alignment between our energy landscape and the existing taxonomy, we further plot the local minima groups as a 2D graph in Fig. 8, which supplements the 1D energy landscape shown in Fig. 7. In Fig. 8, each node represents a local minima group. The edges between nodes denote the energy barriers between the minima groups they connect: Thicker edges indicate lower energy barriers and therefore closer minima groups, and no edge between two nodes means no pathway has been found between the two groups. Nodes with lower barriers between them are placed closer to each other.

Fig. 8a shows that the power grasps and precision grasps are mostly separated from each other, indicating a high energy barrier between the two. One interpretation is that there is no smooth transition between a power grasp and a precision grasp without a non-force-closure grasp along with the transition. Intermediate grasps are scattered around. Nodes that are not colored are grasp types not listed in any existing grasp taxonomy, indicating the manually-defined grasp taxonomy, though carefully collected and designed, still falls short when facing a large variety of grasps.

In Fig. 8b, we draw different types of power grasps in different colors. Only the power grasps close to the precision grasps belong to the power sphere type. This observation

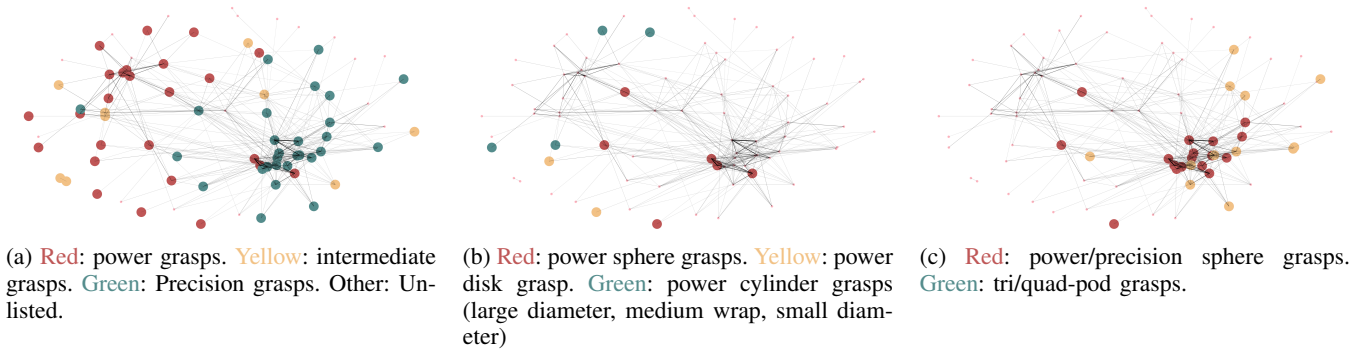


Fig. 8: Alignment between our energy landscape and existing grasp taxonomy [30]. Best viewed in color.

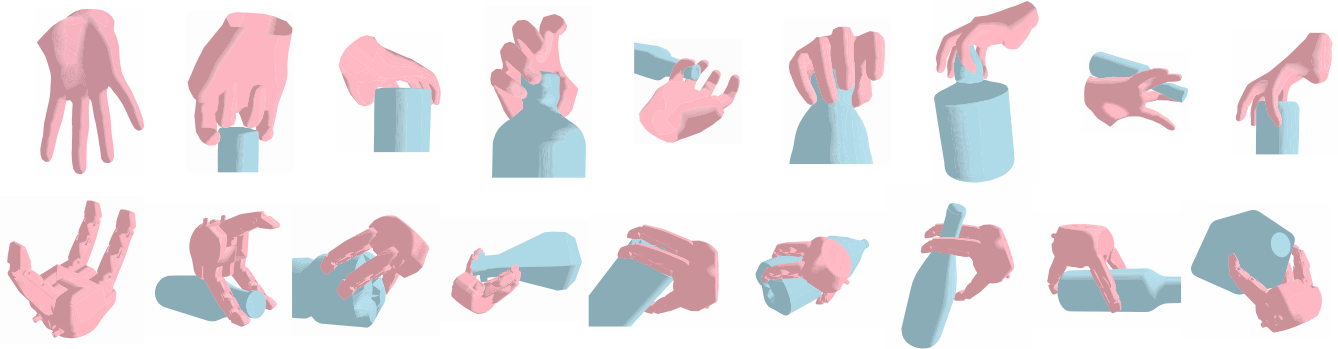


Fig. 9: **Synthesized grasps of different hands using our formulation.** Top: A MANO hand with its thumb removed. Bottom: A Robotiq 3-finger gripper. The left-most figure shows the hand used in each row.

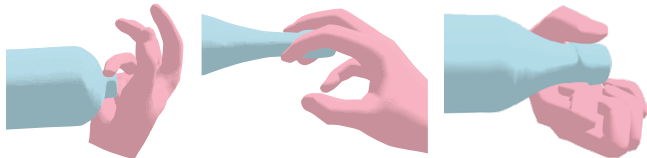


Fig. 10: Examples of novel grasp poses that, to the best of our knowledge, are not included in any grasp taxonomy.

matches our intuition as a power sphere grasp is similar to a precision sphere grasp, with a slight difference in the distance between the object and the palm. In other words, there exists a smooth transition between a precision sphere grasp and a power sphere grasp such that all snapshots along the transition are force-closure grasps. Please refer to [30] for more details on power and precision sphere grasp.

In Fig. 8c, we observe that sphere grasps and tri- or quad-pod grasps are close to each other. This observation is also expected since many sphere grasps can be converted to tri- or quad-pod grasps by merely lifting one or two fingers.

We further demonstrate that our algorithm can find natural but novel and stable grasps in Fig. 10. These grasps are rarely collected in any of the modern 3D grasp datasets (e.g., [5, 24]), since they do not belong to any type as defined in the grasp taxonomy. However, these grasps are valid grasps and could well exist in physical interactions. For example, the left example in Fig. 10 is commonly used when one needs to twist-open a bottle when some of your fingers are occupied or injured. The second example would occur if one is already holding something in the palm while picking up another bottle. These grasp poses happen because

the human hand is excellent in doing multiple tasks simultaneously; they have not been well recognized in the grasp literature as we always assumed otherwise. Such limitation would hinder a robotic hand’s capacity from developing to its full potential. Our method provides possibilities to explore grasps in different types beyond the grasp taxonomy, which is a crucial step toward exploiting the total capacity of a complex hand structure such as human hands.

G. Grasp Synthesis for Arbitrary Hand Structures

Although the above experiments primarily rely on MANO for hand modeling and grasp taxonomy, our method in fact makes no assumption on the hand kinematics except for having a differentiable mapping between pose and shape. As a result, we can synthesize grasps for arbitrary hand so long as there exists such a mapping. In Fig. 9, our method, without modifications, can synthesize grasps of a MANO hand with its thumb removed and a Robotiq 3-finger gripper. Specifically, for the 3-finger gripper, we used a differentiable forward kinematics [38] as the mapping from joint states to the hand shape. These examples demonstrate that our method can explore a wide range of grasps for arbitrary hand structure, which could provide valuable insights for understanding the task affordance of prosthetic or robotic hands, and hands with injuries or disabilities. Our method is also applicable to animations, wherein grasps of non-standard hands or claws are common.

H. Synthesizing Specific Grasp Type

As mentioned in Section IV-B, the choice of contact points on the hand surface primarily determines the grasp type.

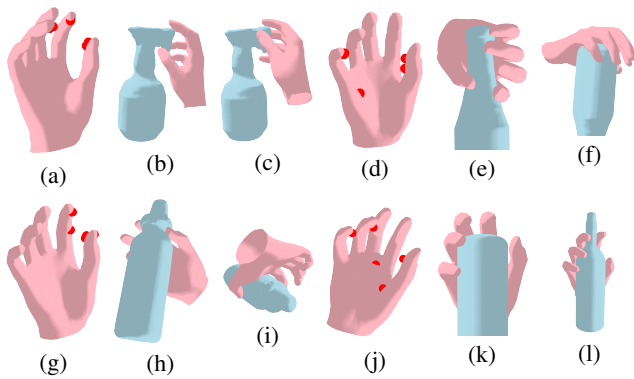


Fig. 11: **Synthesizing specific types of grasping by enforcing contact points.** (a)(d)(g)(j) show the query contact points in red, each followed by two synthesized examples using the queried contact points. Grasp types can be determined by enforcing the choice of contact points on the hand surface.

Hence, specific grasp types can be synthesized by mandating the choice of contact point; see examples in Fig. 11.

VI. CONCLUSION

We formulated a fast and differentiable approximation of the force closure test computed within milliseconds, which enables a new grasp synthesis algorithm. In a series of experiments, we verified that our force closure estimation correctly reflects the quality of a grasp, and demonstrated the proposed grasp synthesis algorithm could generate diverse and physically stable grasps with arbitrary hand structures. The diversity of the generated grasps is validated by its alignment with widely accepted grasp taxonomy.

We believe that exploring different grasp types is crucial for future works of understanding the hand's total functional capacity, whether it is a prosthetic hand, a robotic hand, or an animated character's hand.

REFERENCES

- [1] J. Bohg, A. Morales, T. Asfour, and D. Kragic, "Data-driven grasp synthesis—a survey," *T-RO*, vol. 30, no. 2, pp. 289–309, 2013.
- [2] J. Ponce, S. Sullivan, J.-D. Boissonnat, and J.-P. Merlet, "On characterizing and computing three-and four-finger force-closure grasps of polyhedral objects," in *ICRA*, 1993.
- [3] J. Ponce, S. Sullivan, A. Sudsang, J.-D. Boissonnat, and J.-P. Merlet, "On computing four-finger equilibrium and force-closure grasps of polyhedral objects," *IJRR*, vol. 16, no. 1, pp. 11–35, 1997.
- [4] J.-W. Li, H. Liu, and H.-G. Cai, "On computing three-finger force-closure grasps of 2-d and 3-d objects," *IEEE Transactions on Robotics and Automation*, vol. 19, no. 1, pp. 155–161, 2003.
- [5] O. Taheri, N. Ghorbani, M. J. Black, and D. Tzionas, "GRAB: A dataset of whole-body human grasping of objects," in *ECCV*, 2020.
- [6] S. Baek, K. I. Kim, and T.-K. Kim, "Weakly-supervised domain adaptation via gan and mesh model for estimating 3d hand poses interacting objects," in *CVPR*, 2020.
- [7] K. Karunratanakul, J. Yang, Y. Zhang, M. Black, S. Tang, and K. Muandet, "Grasping field: Learning implicit representations for human grasps," in *3DV*, 2020.
- [8] A. Sahbani, S. El-Khoury, and P. Bidaud, "An overview of 3d object grasp synthesis algorithms," *Robotics and Autonomous Systems*, vol. 60, no. 3, pp. 326–336, 2012.
- [9] A. Rodriguez, M. T. Mason, and S. Ferry, "From caging to grasping," *IJRR*, vol. 31, no. 7, pp. 886–900, 2012.
- [10] D. Prattichizzo, M. Malvezzi, M. Gabbicini, and A. Bicchi, "On the manipulability ellipsoids of underactuated robotic hands with compliance," *Robotics and Autonomous Systems*, vol. 60, no. 3, pp. 337–346, 2012.
- [11] C. Rosales, R. Suárez, M. Gabbicini, and A. Bicchi, "On the synthesis of feasible and prehensile robotic grasps," in *ICRA*, 2012.
- [12] R. M. Murray, *A mathematical introduction to robotic manipulation*. CRC press, 2017.
- [13] A. Saxena, J. Driemeyer, and A. Y. Ng, "Robotic grasping of novel objects using vision," *IJRR*, vol. 27, no. 2, pp. 157–173, 2008.
- [14] M. T. Ciocarlie and P. K. Allen, "Hand posture subspaces for dexterous robotic grasping," *IJRR*, vol. 28, no. 7, pp. 851–867, 2009.
- [15] J. Romero, H. Kjellstrom, and D. Kragic, "Modeling and evaluation of human-to-robot mapping of grasps," in *International Conference on Advanced Robotics*, 2009.
- [16] I. Lenz, H. Lee, and A. Saxena, "Deep learning for detecting robotic grasps," *IJRR*, vol. 34, no. 4-5, pp. 705–724, 2015.
- [17] J. Mahler, J. Liang, S. Niyaz, M. Laskey, R. Doan, X. Liu, J. A. Ojea, and K. Goldberg, "Dex-net 2.0: Deep learning to plan robust grasps with synthetic point clouds and analytic grasp metrics," in *RSS*, 2017.
- [18] S. Levine, P. Pastor, A. Krizhevsky, J. Ibarz, and D. Quillen, "Learning hand-eye coordination for robotic grasping with deep learning and large-scale data collection," *IJRR*, vol. 37, no. 4-5, pp. 421–436, 2018.
- [19] H. B. Amor, O. Kroemer, U. Hillenbrand, G. Neumann, and J. Peters, "Generalization of human grasping for multi-fingered robot hands," in *IRIOS*, 2012.
- [20] Y. Lin and Y. Sun, "Robot grasp planning based on demonstrated grasp strategies," *IJRR*, vol. 34, no. 1, pp. 26–42, 2015.
- [21] S. Brahmabhatt, A. Handa, J. Hays, and D. Fox, "Contactgrasp: Functional multi-finger grasp synthesis from contact," in *ECCV*, 2020.
- [22] P. Grady, C. Tang, C. D. Twigg, M. Vo, S. Brahmabhatt, and C. C. Kemp, "Contactopt: Optimizing contact to improve grasps," in *CVPR*, 2021.
- [23] A. T. Miller and P. K. Allen, "Grasplit! a versatile simulator for robotic grasping," *IEEE Robotics & Automation Magazine*, vol. 11, no. 4, pp. 110–122, 2004.
- [24] E. Corona, A. Pumarola, G. Alenya, F. Moreno-Noguer, and G. Rogez, "Ganhand: Predicting human grasp affordances in multi-object scenes," in *CVPR*, 2020.
- [25] S. P. Boyd and B. Wegbreit, "Fast computation of optimal contact forces," *T-RO*, vol. 23, no. 6, pp. 1117–1132, 2007.
- [26] L. Han, J. C. Trinkle, and Z. X. Li, "Grasp analysis as linear matrix inequality problems," *IEEE Transactions on Robotics and Automation*, vol. 16, no. 6, pp. 663–674, 2000.
- [27] Y. Zheng and C.-M. Chew, "Distance between a point and a convex cone in n -dimensional space: Computation and applications," *T-RO*, vol. 25, no. 6, pp. 1397–1412, 2009.
- [28] H. Dai, A. Majumdar, and R. Tedrake, "Synthesis and optimization of force closure grasps via sequential semidefinite programming," in *Robotics Research*, pp. 285–305, Springer, 2018.
- [29] Y.-H. Liu, "Qualitative test and force optimization of 3-d frictional form-closure grasps using linear programming," *IEEE Transactions on Robotics and Automation*, vol. 15, no. 1, pp. 163–173, 1999.
- [30] T. Feix, J. Romero, H.-B. Schmiemayer, A. M. Dollar, and D. Kragic, "The grasp taxonomy of human grasp types," *IEEE Transactions on Human-Machine Systems*, vol. 46, no. 1, pp. 66–77, 2015.
- [31] J. L. Hintze and R. D. Nelson, "Violin plots: a box plot-density trace synergism," *The American Statistician*, vol. 52, no. 2, pp. 181–184, 1998.
- [32] J. Romero, D. Tzionas, and M. J. Black, "Embodied hands: Modeling and capturing hands and bodies together," *TOG*, vol. 36, no. 6, pp. 1–17, 2017.
- [33] J. J. Park, P. Florence, J. Straub, R. Newcombe, and S. Lovegrove, "Deepsdf: Learning continuous signed distance functions for shape representation," in *CVPR*, 2019.
- [34] A. X. Chang, T. Funkhouser, L. Guibas, P. Hanrahan, Q. Huang, Z. Li, S. Savarese, M. Savva, S. Song, H. Su, *et al.*, "Shapenet: An information-rich 3d model repository," *arXiv preprint arXiv:1512.03012*, 2015.
- [35] M. Hill, E. Nijkamp, and S.-C. Zhu, "Building a telescope to look into high-dimensional image spaces," *Quarterly of Applied Mathematics*, vol. 77, no. 2, pp. 269–321, 2019.
- [36] M. Przybylski, T. Asfour, and R. Dillmann, "Unions of balls for shape approximation in robot grasping," in *IRIOS*, 2010.
- [37] S. Ottenhaus, D. Renninghoff, R. Grimm, F. Ferreira, and T. Asfour, "Visuo-haptic grasping of unknown objects based on gaussian process implicit surfaces and deep learning," in *International Conference on Humanoid Robots (Humanoids)*, 2019.
- [38] G. Sutanto, A. Wang, Y. Lin, M. Mukadam, G. Sukhatme, A. Rai, and F. Meier, "Encoding physical constraints in differentiable newton-euler algorithm," in *Learning for Dynamics and Control*, 2020.